ADVANCED MATERIALS
www.advmat.de

Correlated Rattling of Sodium-Chains Suppressing Thermal Conduction in Thermoelectric Stannides

Takahiro Yamada, Masato Yoshiya,* Masahiro Kanno, Hiroshi Takatsu, Takuji Ikeda, Hideaki Nagai, Hisanori Yamane, and Hiroshi Kageyama*

Tin-based intermetallics with tunnel frameworks containing zigzag Na chains that excite correlated rattling impinging on the framework phonons are attractive as thermoelectric materials owing to their low lattice thermal conductivity. The correlated rattling of Na atoms in the zigzag chains and the origin of the low thermal conductivity is uncovered via experimental and computational analyses. The Na atoms behave as oscillators along the tunnel, resulting in substantial interactions between Na atoms in the chain and between the chain and framework. In these intermetallic compounds, a shorter inter-rattler distance results in lower thermal conductivity, suggesting that phonon scattering by the correlated rattling Na-chains is enhanced. These results provide new insights into the behavior of thermoelectric materials with low thermal conductivity and suggest strategies for the development of such materials that utilize the correlated rattling.

1. Introduction

Thermoelectric materials generate electric power from heat sources with different temperatures, and are thus expected to find numerous applications as independent power sources; e.g., working in small and closed spaces for planetary probes. Such materials can be used as power sources for sensors and wearable devices connected to the Internet of Things (IoT) by exploiting the difference between the room temperature and waste-heat or body temperature.[1] Efficient thermoelectric materials require a large Seebeck coefficient (S), low electrical resistivity (ρ), and low thermal conductivity (κ_{total}). Further, minimizing the lattice component of thermal conductivity ($\kappa_{lattice}$) is of particular importance to obtain a high figure of merit ZT [$= T \times S^2/(\rho \times \kappa_{total})$, where $\kappa_{total} = \kappa_{lattice} + \kappa_{carrier}$] and thus ensure high efficiency because $\kappa_{lattice}$ is the only parameter having no direct physical correlation with S and ρ.[2] Various methods have been employed to reduce the $\kappa_{lattice}$ of materials, including element substitution and the introduction of nano-sized inclusions, grain boundaries, and vacancies.[3-6]

The concept of the phonon glass–electron crystal (PGEC) was introduced by Slack in 1995 as a guide to develop low-$\kappa_{lattice}$ materials.[7] In PGEC materials, atoms contained in relatively large cages of framework structures exhibit large thermal vibration called "rattling" owing to their weak bonding to the atoms of the framework structure. The rattling atoms scatter phonons and thereby reduce $\kappa_{lattice}$ without disturbing carrier transport. Based on this concept, clathrate and skutterudite compounds have attracted considerable attention over the past two decades as low-$\kappa_{lattice}$ thermoelectric materials; these consist of large polyhedral cage

T. Yamada, M. Kanno, H. Yamane
Institute of Multidisciplinary Research for Advanced Material
Tohoku University
2-1-1 Katahira, Aoba-ku, Sendai 980-8577, Japan
E-mail: takahiro.yamada.b4@tohoku.ac.jp

T. Yamada
PRESTO
Japan Science and Technology Agency
4-1-8 Honcho, Kawaguchi 332-0012, Japan

M. Yoshiya
Division of Materials and Manufacturing Science
Graduate School of Engineering
Osaka University
2-1 Yamadaoka, Suita, Osaka 565-0871, Japan
E-mail: yoshiya@mat.eng.osaka-u.ac.jp

The ORCID identification number(s) for the author(s) of this article can be found under https://doi.org/10.1002/adma.202207646.

DOI: 10.1002/adma.202207646

M. Kanno
Department of Metallurgy
Materials Science and Materials Processing
Graduate School of Engineering
Tohoku University
6-6-04 Aramaki Aza Aoba, Aoba-ku, Sendai 980-8579, Japan

H. Takatsu, H. Kageyama
Graduate School of Engineering
Kyoto University
Nishikyo-ku, Kyoto 615-8510, Japan

T. Ikeda
Research Institute for Chemical Process Technology
National Institute of Advanced Industrial Science and Technology (AIST Tohoku)
4-2-1 Nigatake, Miyagino-ku, Sendai 983-8551, Japan

H. Nagai
Research Institute for Energy Conservation
National Institute of Advanced Industrial Science and Technology (AIST)
1-1-1 Higashi, Tsukuba, Ibaraki 305-8565, Japan

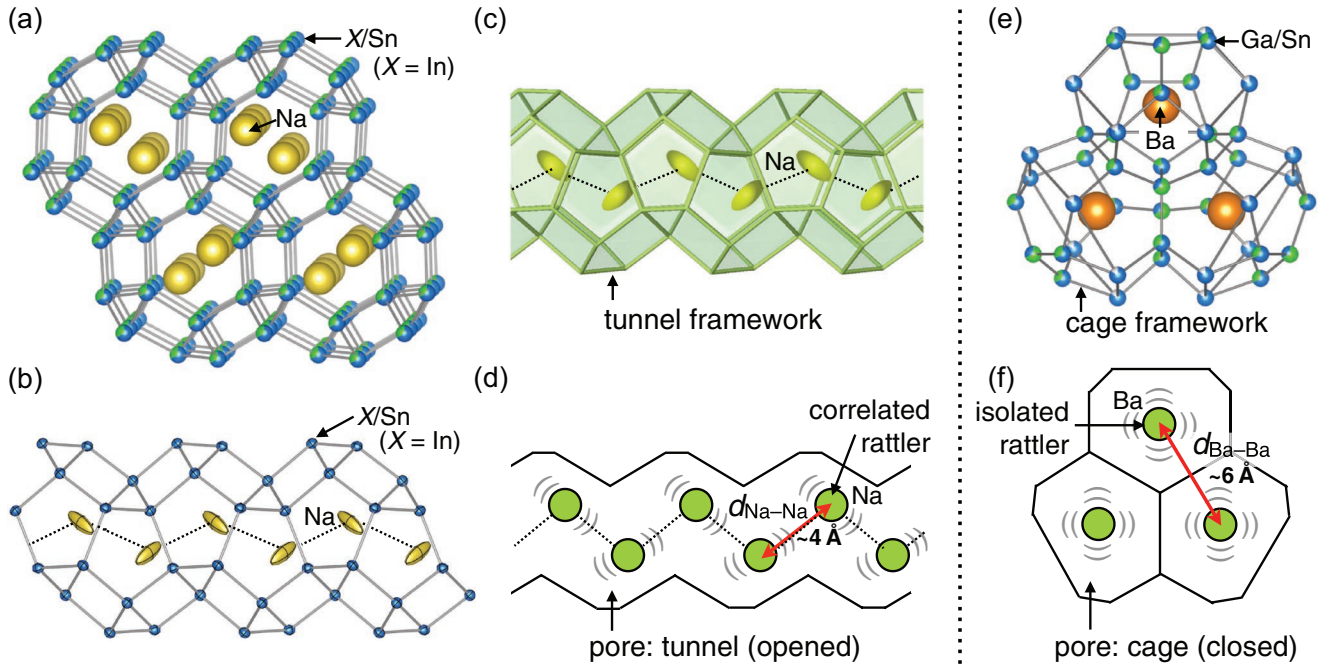

Figure 1. a–d) Conceptual schematics of rattling in Na–(*X*)–Sn compounds having helical tunnel frameworks (*X* = Al, Ga, In, Zn) as compared to e,f) a representative PGEC clathrate compound, β-$Ba_8Ga_{16}Sn_{30}$, having a cage framework structure. a) An overview of the crystal structure of $Na_2In_2Sn_4$, b,c) the helical tunnel containing Na atoms (zigzag chains) as rattlers in $Na_2In_2Sn_4$, and d) a schematic picture of the correlated rattling. e,f) The cages of β-$Ba_8Ga_{16}Sn_{30}$ that enclose Ba atoms as isolated rattlers. The Na atoms in Na–(*X*)–Sn compounds (a–d) exhibit large one-directional thermal motion along the helical tunnel and exhibit shorter inter-atom distances than rattlers isolated in the cages of clathrate compounds (e, f). The thermal ellipsoids in (b) are drawn at 75% probability.

frameworks that encapsulate guest atoms.[8–20] The energy of rattling modes and $\kappa_{lattice}$ of caged compounds, including clathrates and skutterudites, can be reduced by increasing the free space available to guest atoms,[13] while the filling fraction, distribution, and fluctuation of rattlers significantly affect the scattering of low- and mid-frequency phonons, thereby reducing thermal conductivity.[9–11] Rattling Cu atoms with planar 3-coordinate bonding were recently observed in non-caged tetrahedrite compounds such as $(Cu,Zn)_{12}(Sb,As)_4S_{13}$ that exhibit intrinsically low $\kappa_{lattice}$.[21,22] However, the precise mechanism by which rattling phonons reduce $\kappa_{lattice}$ remains under debate.[18–22]

In addition to the cage frameworks found in clathrates and skutterudites, several Sn-based intermetallic compounds ($Na_{2+x}X_{2+x}Sn_{4-x}$ (*X* = Al, Ga, Sn) and Na_2ZnSn_5) exhibit unique "helical tunnel frameworks" comprising Sn atoms and *X* or Zn atoms that host Na atoms in quasi 1D open spaces (**Figure 1**; Figures S1 and S2, Supporting Information).[23–30] Polycrystalline samples of $Na_{2+x}Ga_{2+x}Sn_{4-x}$ (x = 0.19) exhibit excellent thermoelectric properties, with a figure of merit (ZT = 0.98, 295 K) comparable to that of practical Bi_2Te_3-based thermoelectric materials near room temperature (ZT = 1).[27] Two polymorphs (*hP*- and *tI*-phases) of Na_2ZnSn_5 with similar helical tunnel structures exhibit particularly low $\kappa_{lattice}$ values (1.1 and 0.61 W m^{-1} K^{-1}, respectively).[29] The previous studies of the helical-tunnel Na-stannides are summarized in the Supporting Information and the thermoelectric properties of the compounds developed herein are tabulated in **Table 1**. The data indicate helical-tunnel Na-stannides are a promising new class of PGEC materials, despite being unstable in air.[27–29] However, the precise role of the rattling Na atoms in 1D space and the mechanism by which they reduce $\kappa_{lattice}$ remains unclear. It is interesting to understand the role of the rattlers in 1D space and what differentiates these compounds from the compounds with isolated rattling atoms in the cage frameworks in terms of $\kappa_{lattice}$ through a comprehensive examination of several compounds with similar tunnel structures.

Table 1. Relative densities (d_{rel}) and thermoelectric properties of representative polycrystalline samples of the helical-tunnel Na-stannides at 295 K.

Compound	d_{rel} [%]	ρ [mΩ cm]	S [μV K^{-1}]	κ_{total} [W m^{-1} K^{-1}]	$\kappa_{carrier}$ [W m^{-1} K^{-1}]	$\kappa_{lattice}$ [W m^{-1} K^{-1}]	ZT	References
$Na_{1.76}Al_{1.76}Sn_{4.24}$	75	32.4	−222	0.29	–	–	0.15	[28]
$Na_{2.19}Ga_{2.19}Sn_{3.81}$	73	2.38	−209	0.56	–	–	0.98	[27]
$Na_{1.82}Al_{1.82}Sn_{4.18}$	100	4.48	−173	0.58	0.16	0.42	0.34	this study
$Na_{2.19}Ga_{2.19}Sn_{3.81}$	97	1.82	−223	0.99	0.40	0.59	0.82	this study
$Na_2In_2Sn_4$	99	0.99	−98	1.59	0.73	0.86	0.18	this study
hP-Na_2ZnSn_5	98	0.93	−111	1.87	0.77	1.10	0.21	[29]
tI-Na_2ZnSn_5	94	362	−455	0.61	0.00	0.61	0.03	[29]

In this study, the mechanism by which PGEC compounds achieve a low $\kappa_{lattice}$ was elucidated, particularly in relation to the vibrational states of Na and host atoms of Na-stannides with helical tunnel frameworks. The specific heat, crystal structures, and phonon states of five such stannides were analyzed experimentally and by ab initio lattice dynamics. Na atoms are shown to oscillate anisotropically in the tunnel and coupled with each other as in a chain and with the framework lattice. The correlation between Na atoms plays an important role in lowering the $\kappa_{lattice}$ of each compound by triggering the anharmonicity of the phonons in the frameworks.

2. Results and Discussion

2.1. Thermoelectric Properties of Dense Bulk Samples

A densely packed pellet of a polycrystalline specimen is required to obtain a reliable estimate of $\kappa_{lattice}$. The densities of previously prepared samples of the Na-stannides were insufficient with a relative density of ≈75%,[27,28] except for *hP*- and *tI*-Na_2ZnSn_5 where ingots were obtained.[29] Thus, in this study, polycrystalline samples of $Na_{1.82}Al_{1.82}Sn_{4.18}$, $Na_{2.19}Ga_{2.19}Sn_{3.81}$, and $Na_2In_2Sn_4$ with a relative density of 97% or greater were prepared using the press-sintering method (Figure S3, Supporting Information). A monophasic sample can be synthesized reproducibly under the conditions described in Section 4; however, the electronic transport properties of the compounds still exhibit some sample dependence,[27] supposedly owing to different carrier concentrations, especially in samples of $Na_{2.19}Ga_{2.19}Sn_{3.81}$ (Table S1, Supporting Information). Nevertheless, the estimated lattice thermal conductivity of samples with a Lorentz number of 2.45×10^{-8} W Ω K^{-2} is nearly identical, despite slight differences in electronic transport properties of these samples. The thermoelectric properties of representative samples of $Na_{1.82}Al_{1.82}Sn_{4.18}$, $Na_{2.19}Ga_{2.19}Sn_{3.81}$, and $Na_2In_2Sn_4$ are shown in Table 1 and **Figure 2**.

The electrical resistivity (ρ) and thermal conductivity (κ_{total}) of the dense samples of $Na_{1.82}Al_{1.82}Sn_{4.18}$ and $Na_{2.19}Ga_{2.19}Sn_{3.81}$ (Table 1 and Figure 2) showed lower and higher values, respectively, than those of the samples with lower densities in preceding studies.[27,28] These measured values result in the *ZT* value of 0.34 at 295 K and 0.47 at 375 K for $Na_{1.82}Al_{1.82}Sn_{4.18}$ or 0.82 at 295 K and 1.20 at 387 K for $Na_{2.19}Ga_{2.19}Sn_{3.81}$, where the effect of voids in the samples on thermoelectric transport properties is excluded.

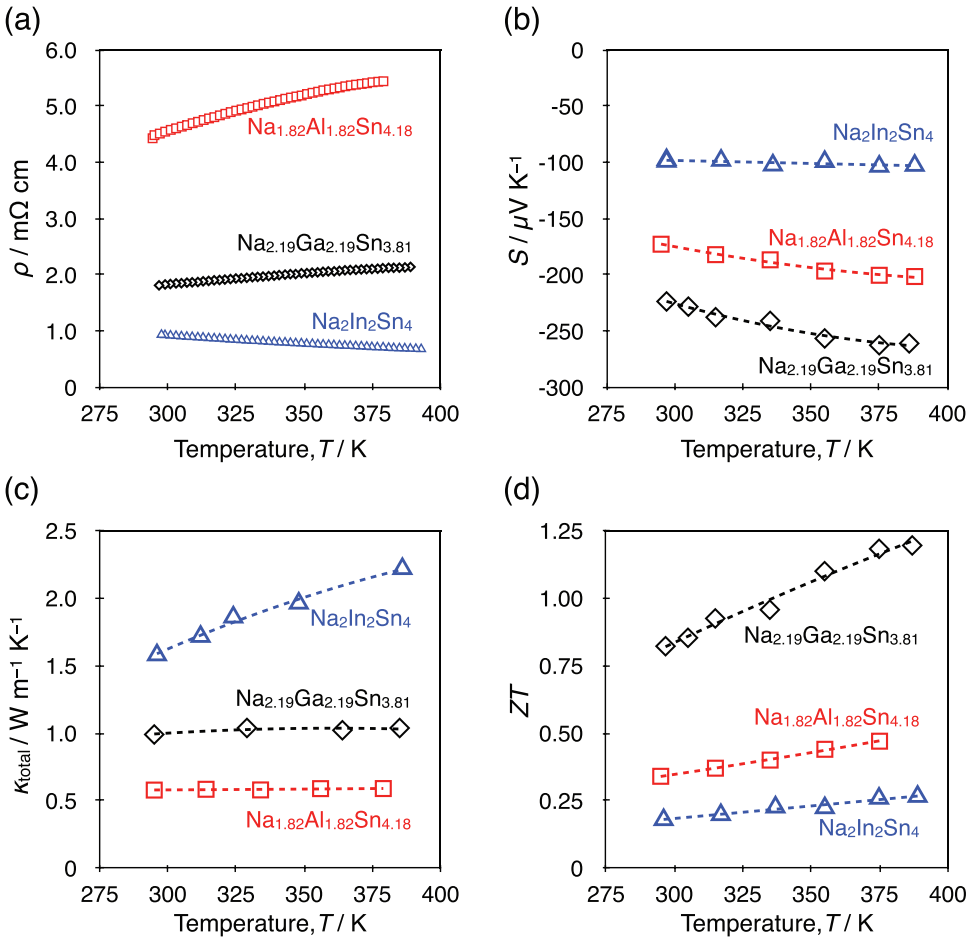

Figure 2. Thermoelectric properties of dense polycrystalline samples of $Na_{1.82}Al_{1.82}Sn_{4.18}$ (red squares), $Na_{2.19}Ga_{2.19}Sn_{3.81}$ (black diamonds) and $Na_2In_2Sn_4$ (blue triangles): a) electrical resistivity, ρ, b) Seebeck coefficient, *S*, c) thermal conductivity, κ_{total}, and d) dimensionless figure of merit, *ZT*, as a function of temperature, *T*.

The $\kappa_{lattice}$ values of $Na_{1.82}Al_{1.82}Sn_{4.18}$, $Na_{2.19}Ga_{2.19}Sn_{3.81}$, and $Na_2In_2Sn_4$ at 295 K are 0.42, 0.59, and 0.86 W m^{-1} K^{-1}, respectively. These values, obtained by subtracting the carrier contribution, $\kappa_{carrier}$, calculated via the Wiedemann–Franz law with a Lorentz number of 2.45×10^{-8} WΩK^{-2} from the total thermal conductivity, are as low as those reported for $Ba_8Ga_{16}Sn_{30}$ clathrates[31–33] and $Al_{0.3}La_{0.5}Co_4Sb_{12}$ skutterudite,[12] with caged frameworks, and tetrahedrites $Cu_{12-x}Tr_xSb_4S_{13}$ (*Tr* = Mn, Fe, Co, Ni, Zn),[21] with non-caged structures. Accordingly, $Na_{2+x}X_{2+x}Sn_{4-x}$ (*X* = Al, Ga, In) are expected to be excellent thermoelectric materials owing to their low $\kappa_{lattice}$ values.

The $\kappa_{lattice}$ of filled and unfilled skutterudite compounds varies significantly depending on the occupancy of rattler atoms encapsulated in the cage-like framework.[9–11] The $\kappa_{lattice}$ of the tunnel compound having a solid-solution phase with the composition $Na_{2+x}Ga_{2+x}Sn_{4-x}$ ($0 \le x \le 0.25$) may decrease as the number of rattlers increases with increasing *x*. However, the $\kappa_{lattice}$ of a sintered $Na_{2+x}Ga_{2+x}Sn_{4-x}$ polycrystalline sample with $x = 0$ (0.60 W m^{-1} K^{-1}) was essentially identical to the $\kappa_{lattice}$ (0.59 W m^{-1} K^{-1}) of the sample with $x = 0.19$ (Table S1, Supporting Information). The effect of the non-stoichiometric composition of rattlers on thermal conductivity for tunnel compounds is expected to be small. Future systematic studies on the compounds with a wider solid solution range may be uncovered in more detail showing the effect of non-stoichiometry.

2.2. Specific Heat Capacities and Low-Temperature XRD Lattice-Dynamics

The specific heat capacities (C_{total}) and atomic displacement parameters (ADPs) obtained from X-ray diffraction (XRD) refinement have been analyzed to determine the vibrational states of the Na and host atoms in the Na-stannide system. Plots of the C_{total}/T^3 of $Na_{1.82}Al_{1.82}Sn_{4.24}$, $Na_{2.19}Ga_{2.19}Sn_{3.81}$, $Na_2In_2Sn_4$, and *hP*- and *tI*-Na_2ZnSn_5 as a function of *T* show broad peaks at ≈10 K (**Figure 3**). Similar plots of clathrate compounds exhibit the same peak that was attributed to the rattling guest atoms.[14,15] The heat capacities of the Na-stannides were analyzed using Equations (1)–(4), assuming that the C_{total} of the stannides could be expressed as a summation of the electronic (C_c), Debye (C_D), and Einstein (C_E) specific heat capacity components in the same way as that of clathrate compounds (**Table 2**).

$$C_{total} = C_c + N_D C_D + N_E C_E \quad (1)$$

$$C_c(T) = \gamma T \quad (2)$$

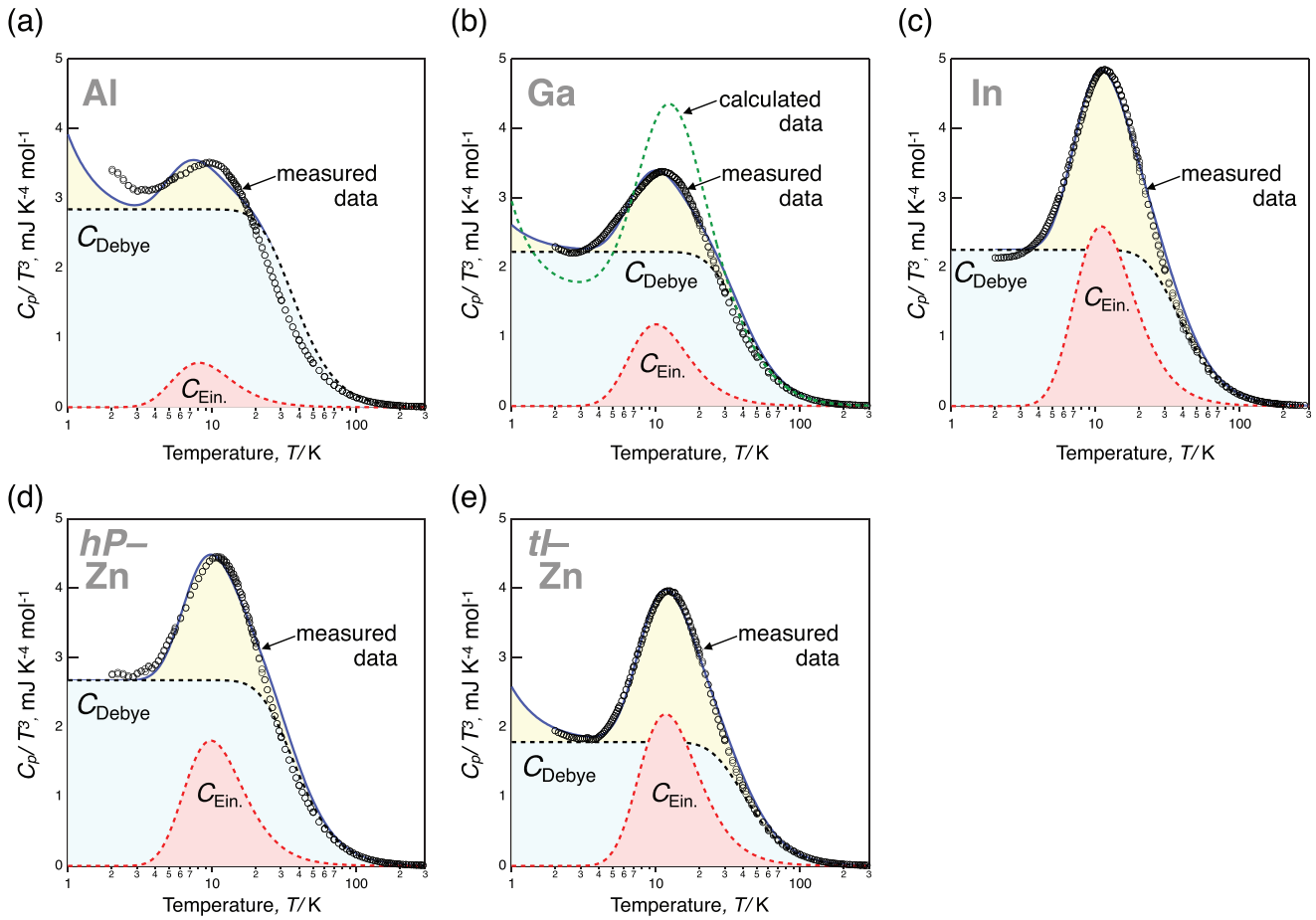

Figure 3. a–e) Specific heat capacity (C_{total}/T^3) of $Na_{1.82}Al_{1.82}Sn_{4.18}$ (a), $Na_{2.19}Ga_{2.19}Sn_{3.81}$ (b), $Na_2In_2Sn_4$ (c), *hP*-Na_2ZnSn_5 (d), and *tI*-Na_2ZnSn_5 (e) as a function of *T*. The blue lines are fitted using Equation (1), and the black and broken red lines show the C_D and C_E components. The green broken line shows the heat capacity of $Na_2Ga_2Sn_4$ calculated by an order model.

Table 2. Characteristic parameters obtained from the analysis of heat capacities and single-crystal XRD patterns of the helical-tunnel Na stannides.

			Heat capacity (polycrystalline)					XRD (single crystal)					
			$C_{electron}$	$C_{Einstein}$		C_{Debye}		Na [U_{aniso_a}]		Na [U_{eq}]		Framework [U_{eq}]	
Compound	N	$3N$	Γ [J K^{-2} mol^{-1}]	N_E	θ_E [K]	N_D	θ_D [K]	Θ_E [K]	d [Å]	Θ_E [K]	d [Å]	Θ_D [K]	d [Å]
$Na_{1.82}Al_{1.82}Sn_{4.18}$	7.82	23.46	1.2×10^{-3}	0.2	38.5	23.2	174	76	0.27	109	0.15	221	0.09
$Na_{2.19}Ga_{2.19}Sn_{3.81}$	8.19	24.57	3.9×10^{-4}	0.8	49.4	23.8	191	76	0.27	110	0.18	204	0.08
$Na_2In_2Sn_4$	8.00	24.00	0[a)]	2.3	54.0	21.7	184	60	0.00	90	0.00	163	0.04
hP-Na_2ZnSn_5	8.00	24.00	0[a)]	1.1	48.2	22.9	177	83	0.31	118[b)]	0.12[b)]	183[b)]	0.10[b)]
tI-Na_2ZnSn_5	8.00	24.00	8.0×10^{-4}	2.4	57.7	21.6	199	72	0.00	108[b)]	0.03[b)]	205[b)]	0.06[b)]

[a)]Small negative γ values of -3.3×10^{-4} J K^{-2} mol^{-1} ($Na_2In_2Sn_4$) and -1.6×10^{-4} J K^{-2} mol^{-1} (*hP*-Na_2ZnSn_5) were initially obtained, but they are theoretically meaningless and indicate that each compound is a degenerate semiconductor with a very small γ value. Therefore, the γ values of $Na_2In_2Sn_4$ and *hP*-Na_2ZnSn_5 were set to 0 in the analysis of their heat capacities. The obtained N_E, N_D, and characteristic temperatures remained essentially unchanged (Table S11, Supporting Information); [b)]Ref. [29]

$$C_D(T) = 3R\left(\frac{T}{\theta_D}\right)^3 \int_0^x \frac{x^4 e^x}{(e^x-1)^2} dx,\ x = \theta_D/T \quad (3)$$

$$C_E(T) = R\left(\frac{\theta_E}{T}\right)^2 \exp\left(\frac{\theta_E}{T}\right)\left(\exp\left(\frac{\theta_E}{T}\right)-1\right)^{-2} \quad (4)$$

Here, γ is the electronic specific heat coefficient; N_D and N_E are the numbers of Debye and Einstein modes, respectively, θ_D and θ_E are the Debye and Einstein temperatures, respectively, and R is the gas constant.

The parameters of Equations (1)–(4) were optimized by fitting the measured C_{total}/T^3 values under the constraint $3N = N_D + N_E$ (Figure 3 and Table 2), where N is the number of atoms in each chemical formula. The N_D and N_E of the clathrate compounds are essentially identical to the number of host and guest atoms per chemical formula multiplied by three, respectively, implying each mode has three degrees of freedom, i.e., 3D motion.[14,15] Interestingly, the N_E values obtained by the same fitting method for the Na-stannides synthesized in this study, ranged from 0.3 to 2.4, significantly lower than the theoretical N_E values (5.46–6.57, assuming three times the number of guest Na atoms as per the chemical formulae). The low N_E values strongly suggest that motion of Na atoms in the helical tunnels is restricted to a single degree of freedom, i.e., one-directional Einstein vibration. Single-crystal X-ray analysis of all helical-tunnel Na-stannides reveals large, one-directional vibrations of Na atoms along the helical tunnels, as demonstrated by the elongation of thermal ellipsoids along the tunnel at the Na site (Figure 1; Figure S2, Supporting Information).[27–29]

The characteristic Debye (Θ_D) and Einstein (Θ_E) temperatures of the host and guest atoms were estimated from the temperature dependence of the equivalent isotropic ADPs (U_{eq}) and anisotropic ADPs (U_{ij}) by fitting with Equations (5) and (6) (Debye and Einstein models, respectively) together with the temperature-independent disorder parameters (d) (Table 2, **Figure 4**; Tables S2–S10, Supporting Information).[13,23]

$$U_{eq,aniso}^{framework}(T) = \frac{3h^2T}{4\pi^2 m k_B \Theta_D^2}\left[\frac{T}{\Theta_D}\int_0^{T/\Theta_D} \frac{x}{\exp(x)-1}dx + \frac{\Theta_D}{4T}\right] + d^2 \quad (5)$$

$$U_{eq,aniso}^{guest}(T) = \frac{h^2}{8\pi^2 m k_B \Theta_E}\coth\left(\frac{\Theta_E}{2T}\right) + d^2 \quad (6)$$

where h and k_B are the Planck and Boltzmann constants, respectively, and m is the mean atomic mass.

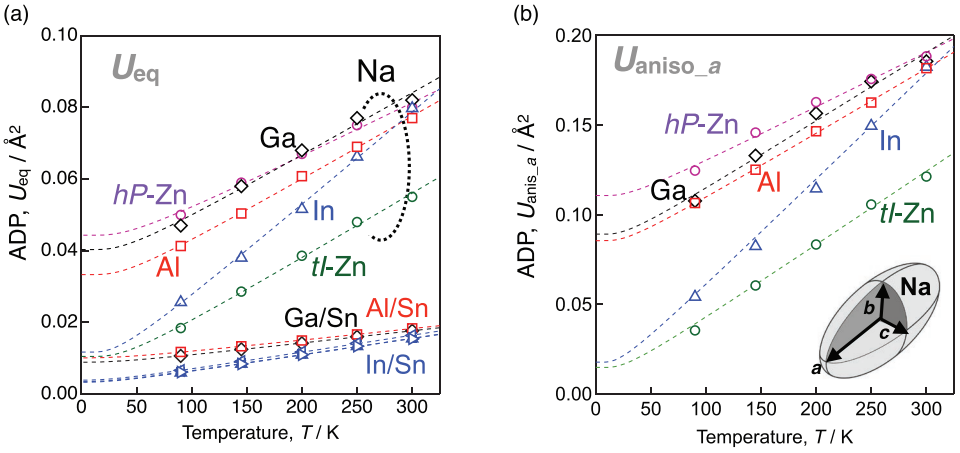

Figure 4. a) Equivalent isotropic displacement parameters (U_{eq}) of the Na and (Al, Ga, or In)/Sn sites of $Na_{1.82}Al_{1.82}Sn_{4.24}$ (red squares), $Na_{2.19}Ga_{2.19}Sn_{3.81}$ (black diamonds), $Na_2In_2Sn_4$ (blue triangles), Na sites of *hP*-Na_2ZnSn_5 (violet circles), and *tI*-Na_2ZnSn_5 (green circles)[29] as a function of temperature. b) Principal axes of anisotropic atomic displacement ellipsoids are along the major axis (U_{anis_a}) of the Na site in each compound against T. The scale of the vertical axis in (b) is twice that in (a).

The Θ_D values of the framework atoms (163–221 K) calculated from U_{eq} are similar to those obtained by specific heat analysis (174–199 K). In contrast, the Θ_E values of Na atoms obtained from the isotropic ADPs (U_{eq}) and from the major-axis component of the anisotropic ADPs, (U_{aniso_a}) were 90–118 K and 72–83 K, respectively, with the latter being closer to the θ_E values obtained using the specific heat (38.5–57.7 K; Table 2). These analyses of the C_{total} and ADP reveal that the Na atoms in the tunnel exhibit anisotropic rattling dynamics with large-amplitude oscillations along the tunnel.

The measured specific heat of compounds having lower $\kappa_{lattice}$ exhibits peak broadening and have a lower intensity. In particular, the specific heat of $Na_{1.82}Al_{1.82}Sn_{4.18}$, which has the lowest $\kappa_{lattice}$, is not adequately reproduced by a simple summation of the electronic, Debye, and Einstein specific heat capacities (Figure 3). This demonstrates that in addition to a reduction in the number of Einstein vibrational modes of Na atoms, the anisotropic vibrational modes deviate from the simple Einstein model (i.e., isolated harmonic modes where atoms do not affect each other). It suggests the existence of interactions among Na atoms, and we will discuss them further in the following sections.

2.3. Calculated Phonon Dispersions and Density of States

To investigate the low $\kappa_{lattice}$ of the helical-tunnel Na-stannides, the phonon dispersions, total and partial densities of states (DOSs), and temperature dependences of the specific heat and ADP of $Na_2Ga_2Sn_4$ were calculated by ab initio lattice dynamics using ordered structure models (**Figure 5**a;Table S12, Supporting Information). Einstein-like peaks are found ≈12.5 meV in the partial DOS of Na where those of Sn and Ga are modest. In addition, the phonon dispersions and partial DOSs (Figure 5b) show many avoided crossings in a wide energy region of 4–13 meV from the Γ point to the M, K, and A points, in which the heat-carrying acoustic-phonon branches are flattened by the interaction between the Na phonons and the acoustic phonons of the framework lattice. Avoided crossings have also been observed in some clathrates and are generally considered an important factor in the reduction of $\kappa_{lattice}$ ($= \frac{1}{3}C_v v^2 \tau$) owing to enhanced phonon scattering caused by a significant decrease in phonon lifetime (τ) and a reduction in the group velocity (v) of the framework phonons near the resonant energies or across a wide energy range.[18–20,34]

The partial DOS (PDOS) of Na of $Na_2Ga_2Sn_4$ exhibits two humps in the low-energy region at 3.9–6.1 meV and 7.1–9.5 meV, both roughly corresponding to those of metallic Na (Figure S4, Supporting Information), overlapped with the partial DOSs of Sn and Ga (Figure 5b). Furthermore, the PDOS of Na is also observed to be overlapped with those of framework atoms up to 25 meV, indicating substantial interactions between the Na atoms and the framework. The temperature dependence of the calculated specific heat capacity (θ_E = 59 K = 5.1 meV) obtained from the phonon structures is in good agreement with the measured specific heat capacity of $Na_{2.19}Ga_{2.19}Sn_{3.81}$ (θ_E = 49 K = 4.2 meV), as shown in Figure 3b. The calculated atomic displacement ellipsoids of Na atoms are also elongated along the direction of the tunnel, in agreement with the ellipsoids refined by X-ray structure analysis (Figure 5a). The Θ_E of Na atoms obtained from the calculated APDs is 74.1 K (=6.6 meV), which is in excellent agreement with that estimated from the measured ADPs of $Na_{2.19}Ga_{2.19}Sn_{3.81}$ (74 K; Figure S5 and Table S13, Supporting Information). These results indicate that Na atoms behave, at least in part, as 1D Einstein-like oscillators. Simultaneously, these atoms are coupled with framework atoms, which are described as swings along the tunnel. The dynamics of the Na atoms scatter the phonons dominated by the framework atoms over a wide energy range via the Na−FW) interaction, thereby reducing $\kappa_{lattice}$.

2.4. Correlated Rattling Examined through Ab Initio Lattice Dynamics

The $\kappa_{lattice}$ of the helical-tunnel Na-stannides varies by a factor of ≈2.5 (0.42–1.1 W m^{-1} K^{-1}). Caged compounds with a larger amount of free space for the rattling of guest atoms typically exhibit smaller Θ_E values, while the guest atom has a larger ADP, resulting in a lower $\kappa_{lattice}$ value; the $\kappa_{lattice}$ of a given

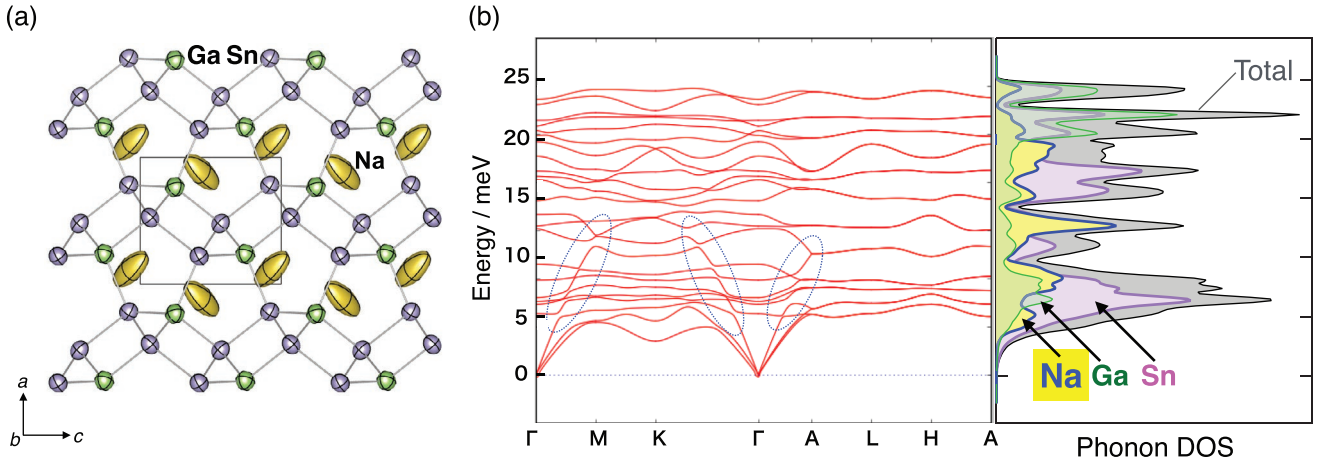

Figure 5. a) Calculated crystal structure of $Na_2Ga_2Sn_4$ at 300 K drawn with 99% probability ellipsoids with an ordered structural model. b) Calculated phonon dispersions (left) and total and partial phonons density of states (right).

compound decreases with Θ_D.[13,35] However, an analysis of the heat capacities and ADPs of each compound (Table 2; Figure S6, Supporting Information) reveals that the $\kappa_{lattice}$ of the helical-tunnel Na-stannides is independent of the Debye and Einstein temperatures (θ_D, Θ_D, θ_E, Θ_E). The $\kappa_{lattice}$ of the tunnel compounds exhibits a strong positive dependence on the interatomic distance (d_{Na-Na}) between Na atoms orderly arranged in the tunnel of $Na_2In_2Sn_4$ and the corresponding distances between Na sites considering their site occupancies in other compounds (Figure S2, Supporting Information), as shown in **Figure 6** and Figure S7 (Supporting Information).

$Na_{1.82}Al_{1.82}Sn_{4.18}$, which has the shortest d_{Na-Na} (3.694(8) Å), also shows the lowest $\kappa_{lattice}$ (0.42 W m^{-1} K^{-1}), while *hP*-Na_2ZnSn_5, which has the longest d_{Na-Na} (3.872(11) Å), exhibits the highest $\kappa_{lattice}$ (1.1 W m^{-1} K^{-1}). These d_{Na-Na} values are similar to that in metallic sodium (3.709 Å)[36] and are as short as 47–65% of the distances between rattling guest atoms encapsulated in the cage compounds (d_{Ba-Ba} in $Ba_8Ga_{16}Sn_{30}$, 5.84 Å (α phase) and 6.08 Å (β phase);[37] d_{Na-Na} in Na_4Si_{23}, 5.70 Å;[38] d_{La-La} in $La_{0.5}Co_4Sb_{12}$, 7.83 Å[12]). This correlation between the $\kappa_{lattice}$ and d_{Na-Na} values of the helical-tunnel Na-stannides remains unchanged even if $\kappa_{lattice}$ values are estimated using other $\kappa_{carrier}$ values, e.g., even when Lorenz numbers described by Kim et al.[39] are used, for example, (Figure S8, Supporting Information).

Despite the clear correlation between lattice thermal conductivity and d_{Na-Na}, however, there is no clear link between these two factors of the correlation from the viewpoint of physics that is a mechanism behind thermal conduction in these compounds and thus the correlation remains a phenomenological explanation at best. To bridge the missing link between thermal conductivity and d_{Na-Na}, thorough examinations of interatomic force constants have been made by means of ab initio lattice dynamics within the harmonic approximation, without using any of the experimentally observed values, except for thermal conductivity, for consistency of the analyses. Second order force constants determine all the phonon states and phonon-related properties within the harmonic approximation. Even though higher order force constants determine thermal conductivity, they are just corrections to the second order force constants for vibrating atoms instead of static atoms at their respective stable positions. Thus, we focus on the second order force constants as their magnitudes to explain: a) interatomic bonds that govern thermal conduction and b) the interatomic bonds that trigger phonon scattering that determines thermal conductivity.

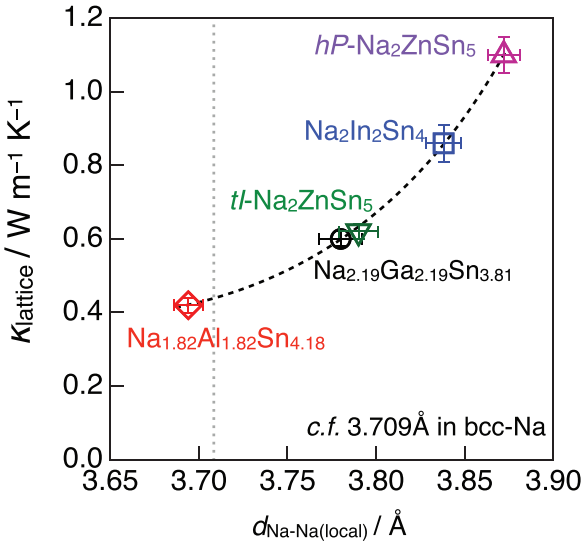

Figure 6. Lattice thermal conductivity ($\kappa_{lattice}$) as a function of the Na–Na interatomic distance (d_{Na-Na}) in helical-tunnel compounds.

Thermal conductivity can be described according to the simplest theory as follows:

$$\kappa_{lattice} = \frac{1}{3} C_V v_G \lambda \quad (7)$$

where C_V, v_G, and λ are heat capacity, group velocity, and phonon mean free path, respectively. As can be seen from Figure S9 (Supporting Information), no clear correlation between the C_V and v_G and the d_{Na-Na} is found, though v_G may decrease with increasing d_{Na-Na}. Here, we intentionally neglect the dependence of v_G on d_{Na-Na} in the following discussion for simplicity and clarity before recalling the dependence of v_G on d_{Na-Na} at the end of the discussion. This leaves phonon mean free path or phonon relaxation time that determines phonon scattering or thermal conductivity in these compounds.

The scalarized force constants for Na—Na bonds, k^{sum}_{Na-Na}, and framework (FW) atoms, k^{sum}_{Na-FW}, and for atoms in the framework, k^{sum}_{FW-FW} are tabulated in **Table 3** together with their respective per-bond values, k^{bond}_{Na-Na}, k^{bond}_{Na-FW} and k^{bond}_{FW-FW}. Since the sum showed negligible dependence on cutoff distance if the nearest neighbor atoms are included, the sums were taken throughout the supercells that are longer than 10 Å along each axis. Although disparities in d_{Na-Na} between experimental and computed values are seen, it can be simply attributed to the use of the ordered models while averaged values among many microscopic states or configurations of atoms by partial occupations were observed in experiments. Interactions among framework atoms measured by k^{sum}_{FW-FW} are much greater than other interatomic interactions given by k^{sum}_{Na-FW} and k^{sum}_{Na-Na} (**Figure 7**a), which manifests that the FW atoms dominate thermal conduction in these compounds.

In contrast to the caged compounds where rattling atoms are rather isolated in cages, k^{bond}_{Na-Na} are greater than that between Na atoms and framework atoms (FW), k^{bond}_{Na-FW} when per-bond values are compared (Table 3), which explains the substantial Debye contribution to specific heats of these compounds discussed above. On the other hand, when sum of these force constants is compared, k^{sum}_{Na-FW}, becomes greater than k^{sum}_{Na-Na} due to greater number of bonds between an Na atom and surrounding FW atoms. The k^{sum}_{Na-FW}, increased with increasing k^{sum}_{Na-Na} as shown in Figure 7b, which explains the influence of phonon states of Na atoms in a zigzag chain onto phonon states of framework atoms, or dynamics of framework atoms that dominate thermal conduction in these compounds. The k^{sum}_{Na-Na} decreases with increasing d_{Na-Na} in the zigzag chain (Figure 7c) that indicates more pronounced Einstein-like behavior with increasing d_{Na-Na} and vice versa.

These explain the reason why the correlation between $\kappa_{lattice}$ and d_{Na-Na} was observed (Figure 6) via dynamic interactions between Na atoms in the zigzag chain with FW atoms that determine $\kappa_{lattice}$. As compared with caged compounds with

Table 3. Sum of the scalarized interatomic force constants and their per-bond maximum that corresponds to the bond at respective nearest neighbor in each compound.

Compounds	Distance [Å] (order model)	Sum of interatomic force constants [eV Å^{-2}]			Interatomic force constants per bond [eV Å^{-2}]		
	d_{Na-Na}	k_{Na-Na}	k_{Na-FW}	k_{FW-FW}	k_{Na-Na}	k_{Na-FW}	k_{FW-FW}
bcc-Na	3.626	3.138					
$Na_2Al_2Sn_4$	3.819	2.638	10.430	73.954	2.050	0.968	7.690
$Na_2Ga_2Sn_4$	3.672	3.118	11.375	70.901	1.936	0.902	7.036
$Na_2In_2Sn_4$	3.987	1.888	10.128	83.016	1.416	0.599	6.173
hP-Na_2ZnSn_5	3.859	2.395	9.676	67.750	2.030	1.065	6.948
tI-Na_2ZnSn_5	3.887	2.301	10.750	67.860	1.734	0.919	7.389

rattlers, these compounds possess an extra degree of freedom to control $\kappa_{lattice}$; interaction within the zigzag chain of Na or separation of the Na atoms. With further increasing d_{Na-Na}, it falls back to the rattling in the caged compounds when FW atoms dominate thermal conduction. Even if we recall the dependences of v_G and k^{sum}_{FW-FW} on d_{Na-Na}, this argument is not changed but rather enhanced and can be explained by phonon conduction in dynamic interaction of phonons in nanometer dimension.[40]

2.5. Overall Pictures of Correlated Rattling of Sodium Chains

Despite the differences among the helical-tunnel Na-stannides, including their crystal systems, the number of atoms in the unit cell, elements forming the framework, and ordering of elements, the observed correlation between $\kappa_{lattice}$ and d_{Na-Na} provides phenomenological evidence supported by underlying physics, i.e., dynamics of chained rattling atoms. Hybrid nature of Einstein–Debye oscillation of Na atoms in the tunnel framework is evidenced by analyses of heat capacity. Anisotropic vibrations of Na atoms are uncovered by low-temperature single-crystal X-ray analysis. Lattice dynamics calculations supported the experimentally observed results and revealed that Na atoms are coupled with each other like a chain and with the framework lattice. Thus, these Na chains are best described as "quasi-1D strongly correlated Na atoms" and explain the clear correlation between $\kappa_{lattice}$ and d_{Na-Na} in helical-tunnel Na-stannides. Unlike rattlers in the caged compounds, Na atoms in the helical tunnel are not spatially isolated and experience stronger forces among themselves as d_{Na-Na} decreases. This modifies phonon propagations through framework atoms, invoking anharmonicity of the phonons, when Na atoms vibrate in a coupled manner in the zigzag chain. The similar is also observed in thermoelectric layered cobaltites.[41]

The conventional caged compounds consisting of closed-cages provide a rattler atom with only one degree of freedom to disturb the acoustic modes dominated by the framework. In contrast, the quasi-1D chains of rattler atoms in the helical-tunnel Na-stannides provide one extra degree of freedom to manipulate framework phonons through interatomic interactions in the chain. The dependence of these interactions on the interatomic Na—Na distance facilitates the precise control of the thermal conductivity of multiple frameworks. Further, the interaction can also be indirectly controlled even with a single choice of elements in a framework. The results indicate a correlated rattling with an extra degree of freedom owing to the interaction of Na atoms in the chain, thus paving the way for an alternative approach to tailor thermal conduction and develop superior thermoelectric materials. Further research into the tunnel compounds with close-packed rattling atoms in a chain and with a wider range of solid-solution compositions including rattling atoms would clarify the effects of the rattler–rattler interactions, rattler–framework interactions, and nonstoichiometry on the thermal transport properties and rattling phenomena.

3. Conclusion

The thermoelectric properties of the tin-based intermetallics with tunnel frameworks containing Na guest atoms

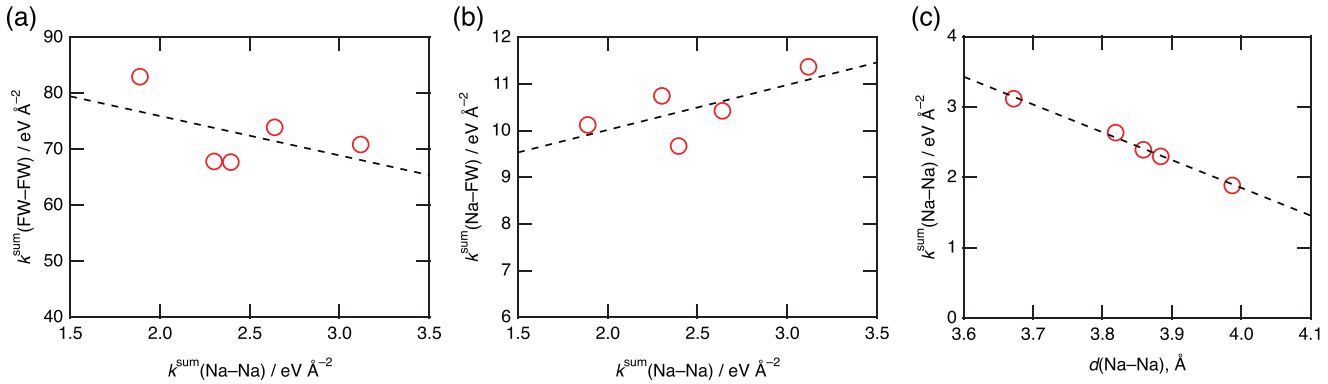

Figure 7. a,b) Interatomic force constants among framework (FW) atoms (a) and between Na atoms and FW atoms (b), and c) the correlation between the interatomic force constants among Na atoms and their separations. The broken lines are just for eyes aid for comparisons using a linear fit.

were investigated using dense bulk samples prepared by pressure-assisted sintering. The Ga-containing stannide ($Na_{2.19}Ga_{2.19}Sn_{3.81}$) showed the highest dimensionless figure of merit (ZT: 0.82 at 295 K and 1.20 at 387 K), while all compounds had low lattice thermal conductivities ($\kappa_{lattice}$: 0.42–1.1 W m^{-1} K^{-1}), which exhibit a strong positive correlation with interatomic distance of Na atoms in the tunnel. X-ray crystallographic and specific heat analyses revealed that Na atoms and framework behave as Einstein-like vibrating rattlers along the tunnel and as a Debye solid, respectively. While ab initio lattice dynamics suggest the presence of significant interactions both among Na atoms and between Na atoms and the framework, the chain-like Na rattlers with large anisotropic oscillations strongly scatter the phonons dominating the thermal conduction in the framework lattice via anharmonicity of the vibrational modes enhanced by the correlation between rattling atoms that become stronger with decreasing inter-rattler distance. These findings provide a deeper understanding of the mechanism by which $\kappa_{lattice}$ is reduced, and thus facilitate the development of the high-performance thermoelectric materials.

4. Experimental Section

Details of Experiments: All manipulations of air-sensitive materials were carried out in an Ar-filled glove box. Ternary stannides of $Na_{2+x}X_{2+x}Sn_{4-x}$ (X = Al, Ga, In) and Na_2ZnSn_5 are unstable in air and gradually decompose into Sn or Sn−−In binary compounds, group 13 and 12 elements, and some sodium hydroxides. Sodium (lump, 99.95%, Nippon Soda), aluminum (powder, 99.99%, Rare Metallic Co. Ltd.), gallium (shot, 99.9999%, Dowa Electronics), indium (lump, 99.999%, Mitsubishi Metal Corporation), zinc (wire, 99.99%, Nilaco Co. Ltd.), tin (shot, ≥99.99%, Rare Metallic and Mitsuwa Chemicals Co., Ltd.), and NaSn powder (prepared in-house) were used as the starting materials. $Na_{2+x}X_{2+x}Sn_{4-x}$ (X = Al, Ga, In) and two polytypes of Na_2ZnSn_5 were synthesized according to previously reported procedures.[27–30] Because $Na_{2+x}Al_{2+x}Sn_{4-x}$ could only be obtained as a solid solution with a less-than-stoichiometric Na content,[28] the most Na-rich composition (x = –0.18, $Na_{1.82}Al_{1.82}Sn_{4.18}$) was chosen because the rattling of Na is an important factor in the reduction of the lattice thermal conductivity. The Na-rich sample (x = 0.19 in $Na_{2.19}Ga_{2.19}Sn_{3.81}$), which gave the highest thermoelectric properties in the previous work on $Na_{2+x}Ga_{2+x}Sn_{4-x}$, was prepared for the same reason.[27] No solid solution with a nonstoichiometric range of compositions was found in Na_2ZnSn_5 or $Na_2In_2Sn_4$.

NaSn, Al, and Sn were weighed in a molar ratio of Na:Al:Sn = 2+x:2+x:4–x, (x = –0.18), and Na, Ga, In, Zn, and Sn were weighed in the molar ratios of Na:Ga:Sn = 2+x:2+x:4–x, (x = 0.19), Na:In:Sn = 2:2:4, and Na:Zn:Sn = 2:1:5. The total amount of the starting materials was 4–6 g.

To synthesize polycrystalline samples of $Na_{1.82}Al_{1.82}Sn_{4.12}$, a mixture of Sn, Al, and NaSn powders was pressed into disc-shaped compacts (φ10–11 × 3–4 mm^3) with a die at a pressure of ≈200 MPa. The compacts were loaded in boron nitride (BN) crucibles (99.5%, φ12 × 18 mm^3, Syowa Denko K. K.), sealed in a stainless steel (SUS) container, and heated at 623 K for 10 h. The obtained samples were pulverized and mixed using an agate mortar and pestle and pressed into compacts again. The compacts were then heated at 623 K for 18–36 h in a crucible sealed in a SUS container, followed by furnace cooling to room temperature. The procedure involving pulverization, mixing, compaction, and heating was performed in triplicate to obtain homogeneous samples. The dense bulk samples (ϕ12 × 3–4 mm^3) were prepared at 573–593 K and 50 MPa for 20 min by pressure sintering.

To synthesize polycrystalline $Na_{2.19}Ga_{2.19}Sn_{3.91}$ samples, Na and Sn were first heated to 873 K for 4 h and then held at this temperature for 2 h in a BN crucible sealed in a SUS container. After heating, Ga was added to the sample in the crucible. The crucible was then sealed again in another SUS container and heated at 973 K for 2 h. Pulverization of the obtained samples, compaction, and heating at 693–713 K for 30–60 h was performed in duplicate. Sample densification was carried out at 673–693 K under 50 MPa for 20 min. The polycrystalline $Na_2In_2Sn_4$ samples were synthesized as follows: the starting materials were heated at 823 K for 10 h and then pulverized, compacted, and heated at 613 K for 18–36 h three times. The dense bulk samples were prepared at 578 K and 50 MPa for 20 min.

Ingots of *hP*-Na_2ZnSn_5 were prepared by heating the starting material at 773 K for 10 h followed by furnace cooling to room temperature. Polycrystalline *tI*-Na_2ZnSn_5 samples were obtained by heating the starting materials at 773 K for 10 h, followed by heating the powder mixture compacts of the obtained samples at 623 K for 36 h twice. The dense bulk samples were prepared at 573 K and 50 MPa for 20 min. The densities of the samples were determined from their weights and volumes. The crystalline phases of the samples were identified by XRD analysis using a Bragg–Brentano type powder diffractometer (Bruker AXS, D2 PHASER, Cu$K\alpha$).

Single crystals of $Na_{2+x}X_{2+x}Sn_{4-x}$ (X = Al, Ga, In) were retrieved from the fragments of the samples prepared from the starting materials with the aforementioned compositions under the following conditions: X = Al, the sample was heated at 673 K and cooled to 653 K for 20 h; X = Ga, the sample was heated at 753 K and cooled to 673 K for 40 h; X = In, the sample was heated at 933 K and cooled to 833 K for 2 h, followed by cooling to 673 K for 400 h. The single crystals were sealed in glass capillaries (outer diameter of 0.5 mm) in a glove box prior to XRD analysis using Mo Kα radiation (λ = 0.71075 Å) on a single-crystal X-ray diffractometer (D8 QUEST, Bruker AXS Inc.) with a multilayered confocal mirror and a CMOS detector. Measurements were made at 300, 250, 200, 145, and 90 K. The XRD data collection, unit-cell refinement, and absorption correction were performed using the Bruker Instrument Service V4.2.0 and APEX3 (Bruker AXS Inc., 2016).[42,43] The crystal structures were refined using full-matrix least-squares on F^2 with the SHELXL-2014 software.[44] Visualization of the crystal structures was performed using the software package VESTA.[45]

The electrical resistivity (ρ), Seebeck coefficient (S), and thermal conductivity (κ) of identical dense bulk samples were measured at 295–393 K by the direct current four-probe method (ρ) and the thermoelectric-power temperature-difference method (S) using a self-made cell, and by the hot disk method[46] (κ) using a commercial instrument (TPS-2500S, Hot Disk AB) with a single-side mode in an Ar-filled glove box. The specific heat capacities of fragments of the dense bulk samples were measured in the range of 2–300 K in a commercial calorimeter (PPMS, Quantum Design, Inc.) by the thermal relaxation method.

Details of Ab Initio Lattice Dynamics: To identify phonon states of Na-chains and frameworks, ab initio lattice dynamics calculations were performed using VASP[47,48] and phonopy[49] codes to obtain optimized atomic configurations and phonon states, respectively. An initial structure model of each compound was constructed such that Na atoms are equally separated and located at the second nearest neighbor site from X-substituted site that corresponds to the configuration showing the minimum total energy, according to preliminary calculations for possibly all the possible configurations for $Na_2Ga_2Sn_4$. Electronic structure calculations were conducted using a plane-wave basis set with a plane wave cut-off energy, k-point mesh grid using Γ-point centered Monkhorst–Pack scheme,[50–52] and real-space mesh grid for fast Fourier transformation to ensure numerical accuracies of 0.1 meV per atom. The mesh grids in reciprocal and real spaces are common to a unitcell containing two Na atoms or the equivalent. The criteria for convergency are 1.0 × 10^{-8} eV per unitcell and 1.0 × 10^{-4} eV Å^{-1} per atom for total energy in electronic structure calculations and structure optimization of both lattice constants and atomic positions to ensure precise evaluations of force constants between atoms. Inner-core electrons are treated as pseudo-potentials using the Projector-augmented wave (PAW) method,[53] with an exception of the 2p electrons of Na, which

are treated as valence electrons. The generalized gradient correction approximation (GGA) formulated by Perew, Berke, and Ernzerhof (GGA-PBE)[54] was used for the exchange-correlation functional, which is known to underestimate bond length and overestimate bond strength for a given atomic configuration. Phonon states were calculated within the harmonic approximation using the finite displacement method[55,56] wherein a displacement of 0.01 Å is given to an atom at a time to obtain the second order force constant matrices and then a dynamical matrix, the solution to which yields phonon eigenvalues and eigenvectors. Phonon partial density of states was calculated with enough fine mesh to ensure convergence with each atom's contribution decomposed without ambiguity. Anisotropic thermal ellipsoids of atomic displacements were calculated based on the cif definition from the phonon eigenvectors and eigenvalues following the scheme developed by Grosse–Kunstleve and Adams.[57]

Values of C_V and ν_G obtained by ab initio lattice dynamics are represented by the constant volume heat capacity of respective compounds at 300 K (Figure S9a, Supporting Information) and group velocity around Γ point that corresponds to sound velocity in these compounds (Figure S9b, Supporting Information), respectively, for simplicity and clarity.

In this study, the second order force constant matrices, Φ_{ij}, were scalarized for ease of comparisons. The force exerted from atom i to atom j, $\vec{F_{ij}}$, is approximated as

$$\vec{F_{ij}} = \Phi_{ij} \cdot \frac{\vec{r_{ij}}}{|\vec{r_{ij}}|} \cdot \Delta r \tag{8}$$

where $\vec{r_{ij}}$ is a vector pointing from atom i to atom j, and Δr is an infinitesimal atomic displacement. From the force, the second order force constants between atom i and atom j, k_{ij}, can be readily calculated as

$$k_{ij} = \frac{|\vec{F_{ij}}|}{\Delta r} \tag{9}$$

within the harmonic approximation. It should be noted that the sum can be readily converted to energies of harmonic oscillators using infinitesimal displacements of atoms, Δr.

Supporting Information

Supporting Information is available from the Wiley Online Library or from the author.

Acknowledgements

The authors would like to thank Ms. Yumi Oikawa and Ms. Reina Kusaka for their assistance in sample preparation and the measurement of thermoelectric properties in a glove box. This work was supported by SAKIGAKE from JST (grant no. JPMJPR151C) and KAKENHI from JSPS (grant nos. JP26288105 and JP20H02820) and was performed under the Cooperative Research Program of "Five-star Alliance" in "NJRC Mater. & Dev."; M.Y. is supported by Grant-in-Aid for Scientific Research from JSPS (grant nos. JP19H05786 and JP20K05062); H.K. and H.T. are supported by CREST of JST (grant no. JPMJCR1421); H.T. is supported by JSPS Core-to-Core Program (grant no. JPJSCCA20200004). T.Y. designed the study and wrote the initial draft of the manuscript. H.Y., M.Y., T.I., H.T., and H.K. contributed to the analysis and interpretation of data and assisted in the preparation of the manuscript. T.Y. and M.K. contributed to the preparation of the samples and characterization of the thermoelectric properties and crystal structures. H.N. characterized the thermal conductivities, H.T. and H.K. collected the specific heat data, H.Y. and T.I. interpreted the measured X-ray diffraction data, and M.Y. calculated and interpreted the phonon dispersion. T.Y., M.Y., H.T., and H.K. thoroughly revised the manuscript. All authors have approved the final version of the manuscript and agreed to be accountable for all aspects of the work to ensure that questions related to the accuracy or integrity of any part of the work are appropriately investigated and resolved.

Conflict of Interest

The authors declare no conflict of interest.

Data Availability Statement

The data that support the findings of this study are available from the corresponding author upon reasonable request.

Keywords

crystal structures, rattling, specific heat, thermoelectric materials, Zintl phases

Received: August 22, 2022
Revised: November 18, 2022
Published online: January 26, 2023

[1] D. M. Rowe, *CRC Handbook of Thermoelectrics*, CRC Press, Boca Raton, FL, USA **1995**.
[2] J. He, T. M. Tritt, *Science* **2017**, *357*, 1369.
[3] D. A. Wright, *Nature* **1958**, *181*, 834.
[4] W. Xu, Y. Liu, B. Chen, D.-B. Liu, Y.-H. Lin, A. Marcelli, *Phys. Chem. Chem. Phys.* **2013**, *15*, 17595.
[5] K. Biswas, J. He, I. D. Blum, C. I. Wu, T. P. Hogan, D. N. Seidman, V. P. Dravid, M. G. Kanatzidis, *Nature* **2012**, *489*, 414.
[6] C. Wood, *Rep. Prog. Phys.* **1988**, *51*, 459.
[7] G. A. Slack, in *CRC Handbook of Thermoelectrics*, (Ed: D. M. Rowe), CRC, Boca Raton, FL, USA **1995**, p. 407.
[8] C. Uher, in *Semiconductors and Semimetals*, Vol. *69*, (Ed: T. M. Tritt), Elsevier, Amsterdam, The Netherlands **2001**, Ch. 5.
[9] G. S. Nolas, J. L. Cohn, G. A. Slack, *Phys. Rev. B* **1998**, *58*, 164.
[10] X. Shi, J. Yang, J. R. Salvador, M. Chi, J. Y. Cho, H. Wang, S. Bai, J. Yang, W. Zhang, L. Chen, *J. Am. Chem. Soc.* **2011**, *133*, 7837.
[11] W. Ren, H. Geng, Z. Zhang, L. Zhang, *Phys. Rev. Lett.* **2017**, *118*, 245901.
[12] M. B. A. Bashir, M. F. Mohd Sabri, S. M. Said, Y. Miyazaki, I. A. Badruddin, D. A. A. Shnawah, E. Y. Salih, S. Abushousha, M. H. Elsheikh, *J. Solid State Chem.* **2020**, *284*, 121205.
[13] T. Takabatake, K. Suekuni, T. Nakayama, E. Kaneshita, *Rev. Mod. Phys.* **2014**, *86*, 669.
[14] D. Huo, T. Sakata, T. Sasakawa, M. A. Avila, M. Tsubota, F. Iga, H. Fukuoka, S. Yamanaka, S. Aoyagi, T. Takabatake, *Phys. Rev. B* **2005**, *71*, 075113.
[15] M. A. Avila, K. Suekuni, K. Umeo, H. Fukuoka, S. Yamanaka, T. Takabatake, *Phys. Rev. B* **2006**, *74*, 125109.
[16] A. Bentien, E. Nishibori, S. Paschen, B. B. Iversen, *Phys. Rev. B* **2005**, *71*, 144107.
[17] B. C. Sales, D. G. Mandrus, B. C. Chakoumakos, in *Semiconductors and Semimetals*, *70*, (Ed: T. M. Tritt), Elsevier, Amsterdam, The Netherlands **2001**, Ch. 1.
[18] M. Christensen, A. B. Abrahamsen, N. B. Christensen, F. Juranyi, N. H. Andersen, K. Lefmann, J. Andreasson, C. R. H. Bahl, B. B. Iversen, *Nat. Mater.* **2008**, *7*, 811.

[19] R. P. Hermann, W. Schweika, O. Leupold, R. Rüffer, G. S. Nolas, F. Grandjean, G. J. Long, *Phys. Rev. B* **2005**, *72*, 174301.
[20] T. Tadano, Y. Gohda, S. Tsuneyuki, *Phys. Rev. Lett.* **2015**, *114*, 095501.
[21] K. Suekuni, C. H. Lee, H. I. Tanaka, E. Nishibori, A. Nakamura, H. Kasai, H. Mori, H. Usui, M. Ochi, T. Hasegawa, M. Nakamura, S. Ohira-Kawamura, T. Kikuchi, K. Kaneko, H. Nishiate, K. Hashikuni, Y. Kosaka, K. Kuroki, T. Takabatake, *Adv. Mater.* **2018**, *30*, 1706230.
[22] W. Lai, Y. Wang, D. T. Morelli, X. Lu, *Appl. Phys. Express* **2015**, *25*, 3648.
[23] W. Blase, G. Cordier, *Z. Naturforsch.* **1988**, *43b*, 1017.
[24] J. T. Vaughey, J. D. Corbett, *J. Am. Chem. Soc.* **1996**, *118*, 12098.
[25] W. Blase, G. Cordier, T. Kniep, T. Schmidt, *Z. Naturforsch.* **1989**, *44b*, 505.
[26] S. Stegmaier, S. J. Kim, A. Henze, T. F. Fässler, *J. Am. Chem. Soc.* **2013**, *135*, 10654.
[27] T. Yamada, H. Yamane, H. Nagai, *Adv. Mater.* **2015**, *27*, 4708.
[28] M. Kanno, T. Yamada, H. Yamane, H. Nagai, *Chem. Mater.* **2016**, *28*, 601.
[29] M. Kanno, T. Yamada, T. Ikeda, H. Nagai, H. Yamane, *Chem. Mater.* **2017**, *29*, 859.
[30] T. Ikeda, T. Yamada, H. Yamane, *J. Phys. Chem. C* **2017**, *121*, 20141.
[31] Y. Saiga, K. Suekuni, S. K. Deng, T. Yamamoto, Y. Kono, N. Ohya, T. Takabatake, *J. Alloys Compd.* **2010**, *507*, 1.
[32] G. S. Nolas, J. L. Cohn, J. S. Dyck, C. Uher, G. A. Lamberton, T. M. Tritt, *J. Mater. Res.* **2004**, *19*, 3556.
[33] Y. Saiga, B. Du, S. K. Deng, K. Kajisa, T. Takabatake, *J. Alloys Compd.* **2012**, *537*, 303.
[34] E. S. Toberer, A. Zevalkink, G. J. Snyder, *J. Mater. Chem.* **2011**, *21*, 15843.
[35] K. Suekuni, M. A. Avila, K. Umeo, H. Fukuoka, S. Yamanaka, T. Nakagawa, T. Takabatake, *Phys. Rev. B* **2008**, *77*, 235119.
[36] F. A. Kanda, R. M. Stevens, D. V. Keller, *J. Phys. Chem.* **1965**, *69*, 3867.
[37] S. Christensen, M. A. Avila, K. Suekuni, R. Piltz, T. Takabatake, M. Christensen, *Dalton Trans.* **2013**, *42*, 14766.
[38] M. Morito, M. Shimoda, H. Yamane, *J. Cryst. Growth* **2016**, *450*, 164.
[39] H. S. Kim, Z. M. Gibbs, Y. Tang, H. Wang, G. J. Snyder, *APL. Mater.* **2015**, *3*, 041506.
[40] S. Fujii, K. Funai, T. Yokoi, M. Yoshiya, *Appl. Phys. Lett.* **2021**, *119*, 231604.
[41] S. Fujii, M. Yoshiya, C. A. J. Fisher, *Sci. Rep.* **2018**, *8*, 11152.
[42] *Bruker Instrument Service*, V4.Vol. *2*.0 Bruker AXS Inc. **2014**, APEX2, SAINT.
[43] APEX3, Bruker AXS Inc., Madison, WI, USA, **2016**.
[44] T. Gruene, H. W. Hahn, A. V. Luebben, F. Meilleur, G. M. Sheldrick, *J. Appl. Crystallogr.* **2014**, *47*, 462.
[45] K. Momma, F. Izumi, *J. Appl. Crystallogr.* **2011**, *44*, 1272.
[46] S. E. Gustafsson, *Rev. Sci. Instrum.* **1991**, *62*, 797.
[47] G. Kresse, J. Furthmüller, *Comput. Mater. Sci.* **1996**, *6*, 15.
[48] G. Kresse, J. Furthmüller, *Phys. Rev. B* **1996**, *54*, 11169.
[49] A. Togo, I. Tanaka, *Scr. Mater.* **2015**, *108*, 1.
[50] A. Baldereschi, *Phys. Rev. B* **1973**, *7*, 5212.
[51] D. J. Chadi, M. L. Cohen, *Phys. Rev. B* **1973**, *8*, 5747.
[52] H. J. Monkhorst, J. D. Pack, *Phys. Rev. B* **1976**, *13*, 5188.
[53] P. E. Blöchl, *Phys. Rev. B* **1994**, *50*, 17953.
[54] J. P. Perdew, K. Burke, M. Ernzerhof, *Phys. Rev. Lett.* **1996**, *77*, 3865; Erratum, *Phys. Rev. Lett.* **1997**, *78*, 1396.
[55] K. Parlinski, Z. Q. Li, Y. Kawazoe, *Phys. Rev. Lett.* **1997**, *78*, 4063.
[56] L. Chaput, A. Togo, I. Tanaka, G. Hug, *Phys. Rev. B* **2011**, *84*, 094302.
[57] R. W. Grosse-Kunstleve, P. D. Adams, *J. Appl. Cryst.* **2002**, *35*, 477.